BIT Numerical Mathematics (2006) 46: 41–59
DOI: 10.1007/s10543-006-0042-7
Published online: 2 March 2006 – © Springer 2006

EXPLOITING RESIDUAL INFORMATION IN THE PARAMETER CHOICE FOR DISCRETE ILL-POSED PROBLEMS*

P. C. HANSEN[1], M. E. KILMER[2] and R. H. KJELDSEN**

[1] *Informatics and Mathematical Modelling, Technical University of Denmark, Building 321, DK-2800 Kgs. Lyngby, Denmark. email: pch@imm.dtu.dk*

[2] *Department of Mathematics, Tufts University, Medford, MA 02155, USA. email: misha.kilmer@tufts.edu*

Abstract.

Most algorithms for choosing the regularization parameter in a discrete ill-posed problem are based on the norm of the residual vector. In this work we propose a different approach, where we seek to use all the information available in the residual vector. We present important relations between the residual components and the amount of information that is available in the noisy data, and we show how to use statistical tools and fast Fourier transforms to extract this information efficiently. This approach leads to a computationally inexpensive parameter-choice rule based on the normalized cumulative periodogram, which is particularly suited for large-scale problems.

AMS subject classification (2000): 65F22, 65R32.

Key words: regularization, discrete ill-posed problems, parameter-choice method, SVD analysis, Fourier analysis.

1 Introduction.

This paper is concerned with the numerical treatment of discrete ill-posed problems, which are highly ill-conditioned linear systems of the form

$$A\,x = b \quad \text{or} \quad \min \|A\,x - b\|_2 \tag{1.1}$$

arising specifically from the discretization of a first-kind Fredholm integral equation. To compute a stable solution to (1.1) one must use regularization, and this involves the choice of a regularization parameter such that the regularized solu-

* Received October 2004. Accepted November 2005. Communicated by Lars Eldén.

** This work was partially supported by grant no. 9901581 from the Danish Natural Science Research Foundation, by NSF grants 0139968 and 0208548 and by CenSSIS (the Center for Subsurface Sensing and Imaging Systems) under the Engineering Research Centers Program of the National Science Foundation (EEC-9986821), and by a travel grant from Observator Julie Marie Vinter Hansens Rejselegat.

tion provides a good fit to the data and, at the same time, is consistent with the user's prior information.

If the singular value decomposition (SVD) of the coefficient matrix can be computed, then it can be used to obtain important information about the regularization problem. In particular, a plot of the singular values and the right-hand side's SVD coefficients is highly useful, e.g., for checking whether the discrete Picard condition is satisfied, and for studying the influence of the noise. These aspects are discussed in detail in Chapter 4 of [8]. The SVD is, however, restricted to small- and medium-sized problems, while it becomes impractical for large-scale problems. Here one must base the analysis on the available quantities: the regularized solution and the corresponding residual.

Many parameter-choice methods have been proposed in the literature, and all of these methods involve residual information in one way or another. A large class of methods are *predictive methods* that seek to provide a regularized solution that predicts the unperturbed right-hand side as well as possible. Among these methods are the discrepancy principle in various incarnations (see §7.2 in [8]), the highly acclaimed method of generalized cross-validation [16], and the more recent ICOMP criterion [15]. Common to all these methods is that they work with the norm of the residual vector; GCV incorporates a scaling that reflects the degrees-of-freedom, and ICOMP incorporates the estimation inaccuracy.

Other parameter-choice methods are *estimation methods* which seek to compute a regularized solution that is as close as possible to the exact solution. Some of these methods involve the computation of additional solutions (see §7.3 in [8]), while others are based on the SVD [13]. All of them also involve the residual norm.

Yet another approach to parameter-choice selection is provided by the L-curve method [6], which seeks to balance the norms of the regularized solution and the corresponding residual. Under certain assumptions this is equivalent to balancing the regularization and perturbation errors in the solution.

While all these method can work well, they tend to work best when there is a sharp transition in the residual from mainly signal to mainly noise – which is often not the case for large-scale problems. One remedy that works for iterative Krylov subspace methods is to choose the regularization parameter in the "projected space" [10], which can also be more efficient when many values of the regularization parameter must be tried.

The main purpose of this work is to go beyond the use of residual norms, and devise a new parameter-choice method that takes advantage of all the information present in the components of the residual vector. In the language of statistics, we want to go beyond the use of the likelihood function as the criterion function. The key theme is that the residual vector contains more information that is worth extracting, and we study which information is relevant for selecting the regularization parameter. We use the (discrete) Fourier transform as our spectral decomposition, since it is the preferred tool in signal processing and because it can be computed efficiently by means of the FFT algorithm. Our approach is inspired by work of Rust [14].

Underlying our work is the notion that, for discrete ill-posed problems arising from first-kind Fredholm integral equations, the singular vectors appear more oscillatory as the corresponding singular values decrease. In order to substantiate this, Section 2 focuses on the spectral properties of the singular functions associated with the underlying continuous integral operator. Section 3 provides further background and notation for the discrete problem, and in Section 4 we study the relations between the Fourier and SVD coefficients of the data and the noise. We note that in our discussion, the SVD is used as an analysis tool only, as the computation of the SVD is to be avoided when solving large-scale problems. In Section 5 we use the insight from Section 4 to design a new parameter-choice method, based on the normalized cumulative periodogram, and in Section 6 we show that our method also works when the noise is correlated with the signal. Finally, in Section 7 we illustrate the use of our method for a large-scale image deblurring problem, and we compare our new method with existing methods by means of a thorough numerical test. Conclusions and future work are the subject of Section 8. Most of our test problems are from the REGULARIZATION TOOLS package [7] with the exception of `gravity` from [9] and an image blurring problem from [12].

2 Relations between Fourier and singular functions.

Although most of our work is presented in the discrete setting, our methods and ideas draw upon certain properties of the underlying continuous problem involving a compact integral operator. Our conclusions for the continuous problem carry over to the discrete setting due to the close relationship between the singular vectors and the singular functions; see, e.g., [5] for details.

In this section we consider the integral operator and the relation between its singular functions and the Fourier functions. In contrast to existing asymptotic results (such as, e.g., [2]), the point of our analysis is to describe behavior that is essentially *non-asymptotic*, since this is what is captured upon discretization. The reader should keep in mind that the material in this section is not intended as a rigorous analysis. Rather, we use some tools from functional analysis to gain insight into non-asymptotic relations between the Fourier and singular functions of the integral operator.

The notation $\langle \cdot, \cdot \rangle$ is used for the $L^2([-\pi, \pi])$ inner product and, in this section only, $\| \cdot \|$ denotes the $L^2([-\pi, \pi])$ norm given by $\|f\|^2 = \langle f, f \rangle$. Define

$$[Kf](x) = \int_\Omega h(x,t)\, f(t)\, dt \quad \text{with} \quad \Omega = [-\pi, \pi].$$

ASSUMPTION 1. Let the kernel h be real and $C^1(\Omega \times \Omega)$ (this can be weakened to piecewise C^1, carrying out the argument below on each piece), and assume that the kernel is non-degenerate.

ASSUMPTION 2. For simplicity, assume $\|h(\pi, t) - h(-\pi, t)\| = 0$; the assumption can be weakened so that this quantity is of the order of the smallest singular value of the integral operator.

It is well known [11] that the operator K is a compact operator $K : L^2(\Omega) \to L^2(\Omega)$. Therefore, there exist $L^2(\Omega)$-orthonormal sequences $u_j(x)$ and $v_j(x)$ and a nonincreasing sequence of positive scalars μ_j with $\lim_{j\to\infty} \mu_j = 0$ such that

$$[Kv_j](x) = \mu_j u_j(x), \quad [K^* u_j](t) = \mu_j v_j(t) \quad \text{almost everywhere}$$

for each integer $j \geq 1$, see §15.4 in [11]. Here, K^* is the adjoint of K, defined by $[K^* f](x) = \int_\Omega h(x,t)\, f(x)\, dx$. The functions u_j and v_j are the left and right singular functions of K.

Now, define the infinite matrix B with rows indexed from $k = -\infty, \ldots, \infty$ and columns indexed by $j = 1, \ldots, \infty$, and with entries $B_{k,j} = |\langle u_j, e^{ikx}/\sqrt{2\pi}\rangle|$. A similar analysis with v_j replacing u_j is omitted. We would like to show the type of phenomenon that we observe in the discrete case (cf. Section 4):

General characterization. The largest entries in the matrix B form a V-shape, with the V lying on the side and the tip of the V located at $k = 0$, $j = 1$.

This means, for example, that the function u_1 is well represented by just the smallest values of k (i.e., low frequencies), and for large values of j the function u_j is well represented only by a small number of the $e^{ikx}/\sqrt{2\pi}$ for some $|k|$ in a band of contiguous integers depending on j. We can think of the singular functions being similar to the Fourier series functions in the sense that large singular values (small j) and their corresponding singular functions correspond to low frequencies, and small singular values (larger j) correspond to high frequencies.

First, we derive an estimate for the terms in the matrix B. We have, for $k \neq 0$,

$$\begin{aligned}
\left\langle u_j, \frac{e^{ikx}}{\sqrt{2\pi}} \right\rangle &= \left\langle \frac{1}{\mu_j} K v_j, \frac{e^{ikx}}{\sqrt{2\pi}} \right\rangle \\
&= \frac{1}{\mu_j} \left\langle v_j, K^* \frac{e^{ikx}}{\sqrt{2\pi}} \right\rangle \\
&= \frac{1}{\mu_j} \int_\Omega v_j(t) \int_\Omega h(x,t) \frac{e^{-ikx}}{\sqrt{2\pi}}\, dx\, dt \\
&= \frac{1}{k\mu_j} \int_\Omega v_j(t) \left\{ (-1)^{k+1} \big[h(\pi,t) - h(-\pi,t) \big] + \int_\Omega \frac{\partial h}{\partial x} \frac{e^{-ikx}}{\sqrt{2\pi}}\, dx \right\} dt
\end{aligned}$$

where the last line is obtained through integration by parts. Therefore, using Assumption 2,

$$\left| \left\langle u_j, \frac{e^{ikx}}{\sqrt{2\pi}} \right\rangle \right| \leq \frac{1}{k\mu_j} \left\| \frac{\partial h}{\partial x}\, \frac{e^{-ikx}}{\sqrt{2\pi}} \right\|. \tag{2.1}$$

It is instructive to show that the term in norm on the right hand side is roughly bounded above by μ_1. By definition of induced operator norms, we know

$$\mu_1 = \max_{\|f\|=1} \|Kf\|$$

and so in particular for $k = \pm 1$ we have $\mu_1 \geq \left\| Ke^{\pm ix}/\sqrt{2\pi} \right\|$. Using integration by parts again, we find

$$\mu_1 \geq \left\| \frac{1}{\sqrt{2\pi}} \frac{\partial h}{\partial x} e^{\pm ix} \right\|.$$

From the Riemann–Lebesque lemma (see, e.g., Theorem 12.5C in [4]) it follows that $\left\| \frac{\partial h}{\partial x}\, e^{-ikx}/\sqrt{2\pi} \right\|$ goes to zero with k. Therefore, we also expect for $|k| > 1$,

$$\mu_1 \gtrsim \left\| \frac{\partial h}{\partial x} \frac{e^{ikx}}{\sqrt{2\pi}} \right\|,$$

so

$$\left| \left\langle u_j, \frac{e^{ikx}}{\sqrt{2\pi}} \right\rangle \right| \lesssim \frac{\mu_1}{k\mu_j}. \tag{2.2}$$

The characterization of the matrix B is a consequence of (2.1), (2.2) and Bessel's and Parseval's inequalities, and is argued by induction on j. The elements in any column of B satisfy

$$\sum_{k=-\infty}^{\infty} |B_{kj}|^2 = \sum_{k=-\infty}^{\infty} \left| \left\langle u_j, \frac{e^{ikx}}{\sqrt{2\pi}} \right\rangle \right|^2 = 1 \tag{2.3}$$

by Parseval's equality, since $e^{ikx}/\sqrt{2\pi}$ is a basis for $L^2(\Omega)$ and $u_j \in L^2(\Omega)$. Note that by orthonormality and Cauchy-Schwarz $|\langle u_j, e^{ikx}/\sqrt{2\pi}\rangle| \leq 1$. Also, since the u_j form an orthonormal set in $L^2(\Omega)$, we have Bessel's inequality

$$\sum_{j=1}^{\infty} |B_{kj}|^2 = \sum_{j=1}^{\infty} \left| \left\langle u_j, \frac{e^{ikx}}{\sqrt{2\pi}} \right\rangle \right|^2 \leq 1, \tag{2.4}$$

showing that for the elements in each row in B, the sum of squares is finite.

Take $j = 1$. Because of (2.1) and (2.2) the terms closest to 1 in magnitude in the first column of B occur only for k very close to $k = 0$. A little calculus on (2.4) using (2.2) shows that for any integer $a > 0$,

$$1 - \frac{2}{a} \lesssim \sum_{k=-a}^{a} \left| \left\langle u_j, \frac{e^{ikx}}{\sqrt{2\pi}} \right\rangle \right|^2.$$

Thus there must be some relatively large terms for k close to 0. So the desired behavior is observed for the base case.

Now consider the jth column of B for any j such that $\mu_j \ll \mu_1$. By (2.2) we know that when k is large enough, say $k > k^*$, the entries B_{kj} will be small. But inequality (2.2) does not tell us about the behavior for k close to zero since $\mu_1/\mu_j \gg 1$. At this point, we know the largest entries occur for indices $|k| \leq k^*$. However, large entries in the jth column cannot occur for rows where $|k| < j$ because of (2.4) – that is, entries large in magnitude have already occurred in

those rows in previous columns, and too many large entries in a row would make the sum greater than one. Therefore, the band of indices for which large entries can occur moves out from the origin as j increases, and we observe a V-shape pattern, as desired.

An analogous argument shows that the matrix involving inner products with v_j and the Fourier functions have a similar pattern.

We note that the results can be strengthened if h is C^m with $\|(\frac{\partial}{\partial x})^{m-1}h(\pi,t) - (\frac{\partial}{\partial x})^{m-1}h(-\pi,t)\| = 0$, for then we have $\left|\left\langle u_j, e^{ikx}/\sqrt{2\pi}\right\rangle\right| \leq c/(\mu_j k^m)$ with c approximately bounded by μ_1.

3 Setting the stage – regularization methods and tools.

Throughout the rest of the paper we consider discretized ill-posed problems of the form (1.1) where the coefficient matrix $A \in \mathbb{R}^{m\times n}$ comes from the discretization of an ill-posed problem. For simplicity we assume that $m \geq n$.

3.1 Tikhonov regularization.

In this paper, we focus our analysis on Tikhonov regularization, in which the regularized solution x_λ solves the problem

$$\min \left\{ \|A\,x - b\|_2^2 + \lambda^2 \|x\|_2^2 \right\}.$$

Recall that if the SVD of A has the form

$$A = U\,\Sigma\,V^T = \sum_{i=1}^{n} u_i\,\sigma_i\,v_i^T$$

with $U \in \mathbb{R}^{m\times m}$, $\Sigma \in \mathbb{R}^{m\times n}$ and $V \in \mathbb{R}^{n\times n}$, then the Tikhonov solution x_λ and its residual r_λ can be expressed in terms of the SVD as

$$x_\lambda = V\,\Psi_\lambda \Sigma^\dagger U^T b, \quad r_\lambda = U\,(I - \Psi_\lambda)\,U^T b, \tag{3.1}$$

where $\Psi_\lambda = \mathrm{diag}(\sigma_i^2/(\sigma_i^2 + \lambda^2))$ and λ is the regularization parameter. However, other regularization schemes, such as regularizing conjugate gradient (CG) iterations which are well-suited to large-scale problems, also lead to solutions that take this form, but with different filter factors.

The tools and methods in this paper are based on the idea of considering the right-hand side as a time series. This is natural when the index in these vectors represents time or some other independent variable, and the perspective can also be useful even when this is not the case. Hence we use terminology and tools from time series analysis; see, e.g., [3] for theory and definitions.

3.2 The discrete Fourier transform.

The matrix F is a unitary matrix that represents the discrete Fourier transform (DFT) such that, for a 1D signal $x \in \mathbb{R}^n$ and a 2D signal $X \in \mathbb{R}^{n\times n}$,

$$\mathrm{dft}(x) = F^H x, \quad \mathrm{dft2}(X) = F^H X\,\mathrm{conj}(F), \tag{3.2}$$

and the elements of F are given by $F_{jk} = n^{-1/2} \exp(2\pi\sqrt{-1}(j-1)(k-1)/n)$ for $i, j = 1, \ldots, n$. Note that F is complex symmetric and therefore $F^H = \text{conj}(F)$. The factor $n^{-1/2}$ in our definition of F differs from standard notation [1], and is introduced to make the transformations to Fourier and SVD bases notationally equivalent. When x is real then it follows from the definition of F that $\text{dft}(x)$ is "conjugate symmetric," i.e.,

$$\text{dft}(x)_{i+1} = \text{conj}\left(\text{dft}(x)_{n-i+1}\right), \quad i = 1, \ldots, q, \tag{3.3}$$

where we have introduced the quantity

$$q = \lfloor n/2 \rfloor + 1.$$

Due to this symmetry relation, for our real problems it therefore always suffices to study the "genuine" parts of the 1D and 2D spectra, computed by

$$F_{\triangleright}^H x \quad \text{and} \quad F_{\triangleright}^H X \,\text{conj}(F_{\triangleright}) \quad \text{with} \quad F_{\triangleright} = F(:, 1\colon q).$$

3.3 The normalized cumulative periodogram (NCP).

If x is a vector of length n, then the *periodogram* – or power spectrum – of x is defined as the vector $p = |F_{\triangleright}^H x|^2$ of length q with elements

$$p_k = |\text{dft}(x)_k|^2, \quad k = 1, \ldots, q \tag{3.4}$$

(we omit a scaling factor $2/n$ that is sometimes found in the statistical literature). The *normalized cumulative periodogram* (NCP) for x is then defined as the vector $c(x)$ of length $q-1$ with elements

$$c(x)_k = \frac{\|p(2\colon k+1)\|_1}{\|p(2\colon q)\|_1}, \quad k = 1, \ldots, q-1. \tag{3.5}$$

Note that the first component of p (the DC component of x) is not involved in the definition of the NCP. Therefore $c(x)_k$ represents the normalized integral of the power spectrum from frequencies 1 to k.

For a 2D signal represented by the $n \times n$ matrix X, we define the NCP in a similar manner. Let the $q \times q$ matrix $P = |F_{\triangleright}^H X \,\text{conj}(F_{\triangleright})|^2$ be the power spectrum of X with elements given by

$$P_{k\ell} = |\text{dft2}(X)_{k\ell}|^2, \quad k, \ell = 1, \ldots, q, \tag{3.6}$$

and let $\text{vec}(P)$ denote the vector obtained by stacking all the columns of P into a vector of length q^2. Next we need to reorder these elements in order of increasing spatial frequency, and for this purpose we introduce the $q \times q$ matrix Ξ with elements $\Xi_{ij} = i^2 + j^2$ and the $q^2 \times q^2$ permutation matrix Π such that the elements of $\Pi\,\text{vec}(\Xi)$ appear in nondecreasing order. Then the vector

$$\hat{p} = \Pi\,\text{vec}(P) \tag{3.7}$$

holds all the power spectrum elements in order of increasing spatial frequency, and we define the NCP for X as the vector $c(X)$ of length $q^2 - 1$ with elements

$$c(X)_k = \frac{\|\hat{p}(2\colon k+1)\|_1}{\|\hat{p}(2\colon q^2)\|_1}, \quad k = 1, \ldots, q^2 - 1. \tag{3.8}$$

Again, the DC component of X does not contribute to the NCP.

3.4 White noise.

A noise signal e is called *white noise* when it is a zero-mean random vector whose elements are uncorrelated and have the same standard deviation η. The covariance matrix for e is thus given by

$$\mathrm{Cov}(e) = \eta^2 I. \tag{3.9}$$

Such random vectors can, for example, be generated by the Matlab commands `e = eta*randn(m,1)` and `e = eta*sqrt(3)*(2*rand(m,1)-1)`. Now consider the covariance matrix for the DFT of e:

$$\mathrm{Cov}(F^H e) = F^H \mathrm{Cov}(e)\, F = \eta^2\, F^H F = \eta^2\, I.$$

Since the diagonal of $\mathrm{Cov}(F^H e)$ is equal to the expected value of the (scaled) power spectrum we see that all frequencies have the same expectation. In other words, in a white-noise signal the expected power spectrum is flat – hence the name – and the expected values of the elements in the NCP lie on a straight line between (0,0) and $(q, 1)$.

Note that since U is an orthogonal matrix, by a similar argument we also have $\mathrm{Cov}(U^T e) = \eta^2 I$, and thus all SVD-frequencies have the same expectation. Thus $\mathrm{Cov}(F^H e) = \mathrm{Cov}(U^T e)$ when e is white noise. This simply means that $F^H e$ and $U^T e$ behave statistically in the same manner, even though $F^H e \neq U^T e$ in general. Therefore any statistical test for white-noise should behave the same way when applied to either of these two quantities.

When testing a vector for white noise, the NCP of the vector should lie within the Kolmogorov–Smirnoff limits of the straight line. If the significance level is 5 percent then the limits are $\pm 1.36\, q^{-1/2}$ in the 1D case, and $\pm 1.36\, q^{-1}$ in the 2D case; see p. 363 in [3].

4 The similarity of SVD and Fourier coefficients.

In this section we are concerned with additive white noise, i.e., the right-hand side b is of the form $b = \bar{b} + e$, where $\bar{b}$ is the exact right-hand side and e is a white noise signal. We note that this includes the case where e is non-white and an estimate of its covariance matrix is known, such that the noisy signal can be pre-whitened by multiplication with the inverse of the Cholesky factor of the covariance matrix.

In addition to the noise vector e being white, we shall also assume that the vectors $\bar{b}$ and e are statistically independent time series; that is, $E(\bar{b}e^T) = 0$,

where E is the expectation. This assumption implies that the covariance matrices of b and e are identical, $\mathrm{Cov}(b) = \mathrm{Cov}(e)$.

We shall frequently refer to $\bar{b}$ as the signal component. It is important to recall that for the class of problems we consider, this vector originates as the result of an integral operator acting on some function, and due to the smoothing effect of the integration, this vector is bound to be dominated by low-frequency components. In other words, the power spectrum of $\bar{b}$ tends to have larger values at low frequencies than at high frequencies. Thus the signal component $\bar{b}$ behaves spectrally different from the white noise component e, which gives us hope that we can distinguish the two components.

Now consider the Fourier coefficients $\mathrm{dft}(b)$ of the noisy signal vector $b = \bar{b} + e$. As long as the signal-to-noise ratio is not too small, the low-frequency components of b will be dominated by contributions from $\bar{b}$, while at higher frequencies we can expect the Fourier components to be dominated by contributions from e. Thus, the overall behavior is such that the resulting power spectrum of b first decays and then rolls off at the noise level η^2.

Precisely the same behavior is observed in the right-hand side's SVD components, i.e., the elements in the vector $U^T b = U^T \bar{b} + U^T e$. Due to the relation $\mathrm{Cov}(U^T e) = U^T \mathrm{Cov}(e)\, U = \eta^2 I$ we see that the vector $U^T e$ is also white noise. Moreover, since for the class of discrete ill-posed problems we are considering the singular vectors u_i have more oscillations as the index i increases, and since $\bar{b}$ is dominated by low-frequency components, we know that the quantities $|u_i^T \bar{b}|$, on the average, will decrease. The overall picture is that for small values of the index i the SVD components will be dominated by $u_i^T \bar{b}$ and thus decrease in magnitude, while for larger indices the SVD components will be dominated by $u_i^T e$ and thus level off at the noise level.

Figure 4.1 shows the quantities σ_i, $|\beta_i| = |u_i^T b|$, and $|\phi_i| = |(F_\triangleright^H b)_i|$ against one another as a function of i for test problem `gravity(128,2)` with noise level $\|e\|_2 / \|\bar{b}\|_2 = 10^{-2}$. Clearly ϕ_i decays in a manner similar to β_i, with $|\phi_1|$ and $|\beta_1|$ virtually indistinguishable.

5 The NCP parameter-choice method.

Let us consider problems arising from discretizations of 1D problems in the form of Fredholm integral equations of the first kind, where the solution x represents a 1D signal (we consider 2D signals in Section 7). To illustrate the relationship between the behavior of the Fourier coefficients $\mathrm{dft}(b) = F^H b$ and the SVD coefficients $U^T b$, it is instructive to consider the Fourier coefficients of the singular vectors. That is, we consider the vectors $F^H u_i$ for $i = 1, \ldots, m$.

Figure 5.1 shows plots of the absolute values of the elements of $F^H U$ for three model problems `deriv2`, `phillips` and `gravity` of size $n = 100$. The first problem (computation of the second derivative) illustrates an ideal situation, because the singular functions are the sine functions. For the other two problems, we see that each singular vector u_i contains Fourier components only in a small frequency range, and the dominating frequency shifts from low to high as the

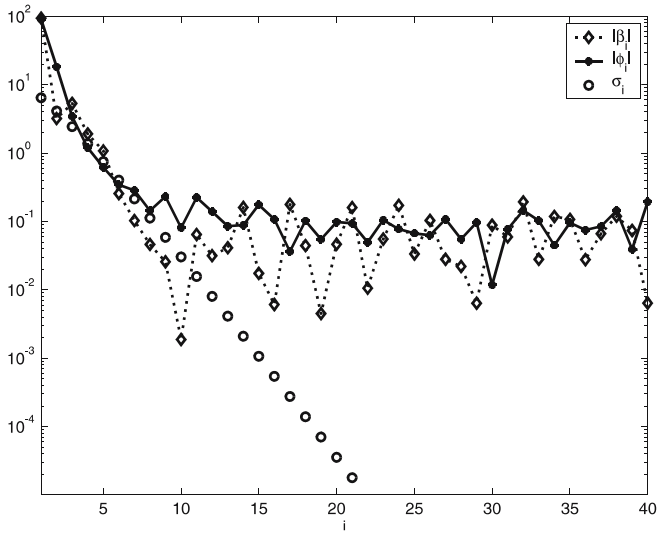

Figure 4.1: Plot of the first 40 value of σ_i, $|\beta_i| = |u_i^T b|$, and $|\phi_i| = |(F_\triangleright^H b)_i|$ as a function of i for `gravity(128,2)`. The noise level is $\|e\|_2/\|\bar{b}\|_2 = 10^{-2}$.

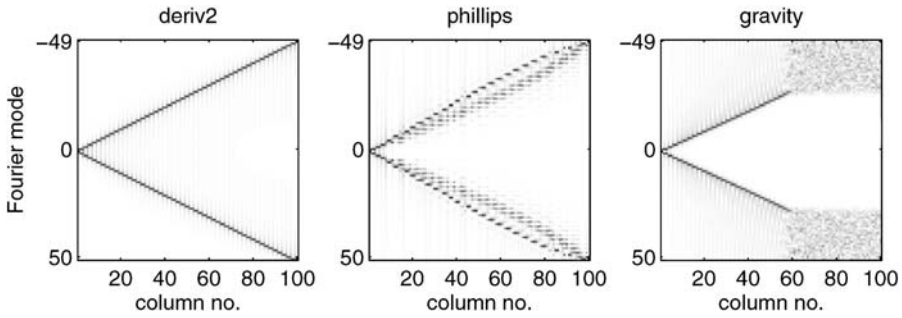

Figure 5.1: Plots of the absolute values of the matrices $F^H U$, where F is the Fourier matrix and U is the left singular matrix of the coefficient matrix, for three different model problems `deriv2`, `phillips` and `gravity` with $n = 100$. The frequency axis is such that the zero frequency (the DC component) is in the middle. The last 40 columns of U for `gravity` correspond to singular values at the machine precision level, and are therefore not well determined.

index i increases. Not surprisingly, since these problems come from discretized first-kind Fredholm integral equations, this phenomenon is consistent with the general characterization outlined in Section 2.

We conclude that the SVD basis indeed provides a kind of spectral decomposition very similar to the decomposition in the Fourier basis for this class of discrete ill-posed problems, as explained in Section 2. This is particularly useful in those situations where the Fourier basis does not naturally provide a basis, e.g., when data cannot be considered as samples of a periodic function on a regular grid.

Next we consider the residual vectors corresponding to regularized solutions. When the solution is over-regularized (i.e., λ is too large) then we see from (3.1), as well as Figure 4.1, that the residual is dominated by the signal components $|u_i^T \bar{b}|$ corresponding to small indices i. As λ decreases the solution becomes less regularized, and the residual will eventually be dominated by the noise components $|u_i^T e|$ corresponding to large indices i (when λ is too small and the solution is under-regularized).

Consider now the noise component in the residual vectors, expressed in both the SVD and Fourier bases. For Tikhonov regularization we have

$$U^T r_\lambda = (I - \Psi_\lambda)\, U^T b \quad \text{and} \quad F^H r_\lambda = F^H U\, U^T r_\lambda,$$

and thus

$$\mathrm{Cov}\big(U^T r_\lambda\big) = \eta^2 (I - \Psi_\lambda)^2, \quad \mathrm{Cov}\big(F^H r_\lambda\big) = \eta^2\, F^H U\, (I - \Psi_\lambda)^2 U^T F,$$

where $(I - \Psi_\lambda)^2 = \mathrm{diag}(\lambda^4/(\sigma_i^2 + \lambda^2)^2)$. We see that as long as λ is not too small, then the residual's noise component is *white-noise like*, in the sense that it is slightly high-pass filtered white noise with the lowest frequencies removed.

Due to the similarities between the SVD and Fourier bases for the class of discrete ill-posed problems that we consider, we conclude that when λ is large the residual vector will resemble a signal dominated by low-frequency components, both in the Fourier and the SVD basis. For smaller λ, when the signal component of the residual is no longer dominating, the residual is white-noise like and resembles slightly high-pass filtered white noise.

We define the "optimal" regularization parameter as the parameter which gives a regularized solution that has minimum relative error in the 2-norm. The conclusion based on the preceding discussion is that any test for white noise that relies on the Fourier components of the residual, particularly tests based on the NCP, will detect white noise at the optimal regularization parameter, provided the optimal parameter is not so small that the residual's noise component contains very high-pass filtered white noise. However, in practice, the noise-levels are such that the optimal parameter is not going to be that small and such a test should therefore be appropriate.

The key idea in our parameter-choice algorithm is therefore to choose the regularization parameter for which the residual vector changes from being dominated by remaining signal to being white-noise like. Once all spectral components with magnitude above the noise-level have been extracted, by the argument above we see that this is when the residual most resembles a white-noise distribution. Figure 5.2 illustrates the changes in the NCP as a function of regularization parameter λ, for the test problem `deriv2(256,2)` with noise level $\|e\|_2/\|\bar{b}\|_2 = 10^{-2}$. Clearly, for large values of λ the residual is dominated by low-frequency information, while for small values it is dominated by high-frequency information. For the fifth choice, $\lambda = 2.7 \cdot 10^{-3}$, the NCP resembles a straight line and thus the residual vector resembles white noise.

The computational tool for deciding if the residual vector is white is the Kolmogorov–Smirnoff test in the NCP. That is, if the actual NCP lies within

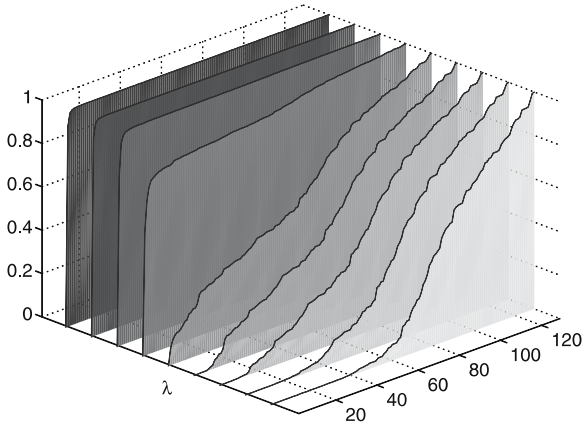

Figure 5.2: Plots of NCPs for various Tikhonov regularization parameters λ, for the test problem `deriv2(128,2)` with noise level $\|e\|_2/\|\bar{b}\|_2 = 10^{-5}$. The values of λ used for this plot are, from left to right: 1, 0.23, $5.2 \cdot 10^{-2}$, $1.2 \cdot 10^{-2}$, $2.7 \cdot 10^{-3}$, $6.2 \cdot 10^{-4}$, $1.4 \cdot 10^{-4}$, $3.3 \cdot 10^{-5}$, 10^{-5} (going from over-smoothing to under-smoothing).

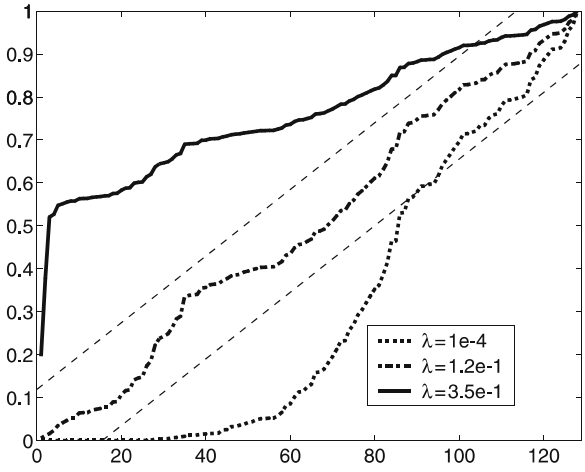

Figure 5.3: NCPs for test problem `phillips(256)` with noise level $\|e\|_2/\|\bar{b}\|_2 = 5 \cdot 10^{-3}$ and for three values of λ. The two dashed lines are the Kolmogorov–Smirnoff limits.

the Kolmogorov–Smirnoff limits of the theoretical one, the conclusion is the acceptance of the hypothesis that the residual is white noise.

To further illustrate the use of the NCP and the Kolmogorov–Smirnoff limits, Figure 5.3 shows three NCPs for the test problem `phillips(256)` with noise level $\|e\|_2/\|\bar{b}\|_2 = 5 \cdot 10^{-3}$ for three values of λ. For the large value $\lambda = 0.35$, essentially only a single Fourier component has been extracted from the right-hand side, and the residual is dominated by low-frequency information from the signal. For the small value $\lambda = 10^{-4}$ about 40 Fourier components have been extracted, leaving mainly high-frequency information in the residual. In

both cases, the residual is not white-noise like, and large parts of the NCPs fall outside the Kolmogorov–Smirnoff limits. For $\lambda = 0.19$, however, the NCP is completely within the limits and the residual can safely be considered to be white-noise.

Often there will be several regularized solutions whose residuals satisfy the Kolmogorov–Smirnoff test – this is not a flaw of the theory, but rather reflects that there is often not a single "optimal" solution. If one needs a single regularization parameter then we have two choices.

1. Among the regularization parameters for which the residual satisfies the Kolmogorov–Smirnoff test in the NCP, choose the one that gives the most regularization (to be on the safe side). I.e., for Tikhonov regularization choose the largest λ for which r_λ satisfies Kolmogorov–Smirnoff test.
2. Choose the regularization parameter for which the residual vector most resembles white noise. To measure this, compute the largest difference, in absolute value, between the estimated and the theoretical NCP, and choose the regularization parameter that minimizes this difference. I.e., for Tikhonov regularization, choose the λ that minimizes the function

$$\mathcal{N}(\lambda) = \|v - c(r_\lambda)\|_1, \tag{5.1}$$

where v is a vector with elements $v_i = i/d$, where $d = q-1$ for a 1D problem and $d = q^2 - 1$ for a 2D problem.

Both variants of the NCP-based parameter choice method are well suited for any regularization method where the residual vector is readily available, including regularizing iterative methods, as we show in the numerical results section.

Furthermore, we note that the NCP-based parameter-choice method is computationally attractive because the core computational tool is the fast Fourier transform, making the method particularly suited for large-scale problems.

We emphasize that the NCP can be used to provide more than a regularization parameter choice. The overall shape of the NCP provides important qualitative information, in that it gives *insight* into how the spectral components are extracted as the regularization parameter varies. Again, this relies on the close relationship between the Fourier and SVD coefficients.

6 Signal-correlated noise.

In this section we study the kind of noise which is encountered when the perturbation in each data is proportional to the signal, i.e., when the elements of the noisy signal e_b are given by

$$b_i = \bar{b}_i(1 + e_i), \quad i = 1, \ldots, m,$$

where e_i are again elements of a zero-mean white-noise vector. Hence, in this case the noise vector is generated by the model

$$e_b = \mathrm{diag}(\bar{b})\, e, \tag{6.1}$$

where e denotes zero-mean white noise with standard deviation η and which is independent of $\overline{b}$. Thus, the covariance matrix for e_b is $\eta^2\,\mathrm{diag}(\bar{b})^2$. The covariance matrix for the DFT of e_b is therefore

$$\mathrm{Cov}\big(\mathrm{dft}(e_b)\big) = \mathrm{Cov}\big(F^H e_b\big) = \eta^2\, F^H \mathrm{diag}(\bar{b})^2 F. \tag{6.2}$$

Now recall that any $m \times m$ circulant matrix C whose first column is $c = C_{:,1}$ has the eigenvalue decomposition $F\,\mathrm{diag}(m^{1/2}F^H c)\,F^H$, see [9], and therefore $\mathrm{Cov}(F^H e_b)$ is a circulant matrix whose first column is the vector $F\,(\bar{b}_1^2, \ldots, \bar{b}_m^2)^T$. Now using that $F^H = \mathrm{conj}(F)$ and that $\bar{b}$ is real, we conclude that the first column of $\mathrm{Cov}(F^H e_b)$ is given by

$$\big(\mathrm{Cov}\big(F^H e_b\big)\big)_{:,1} = \eta^2\, m^{-1/2}\, \mathrm{conj}\big(F^H \big(\bar{b}_1^2, \ldots, \bar{b}_m^2\big)^T\big), \tag{6.3}$$

where $F^H(\bar{b}_1^2, \ldots, \bar{b}_m^2)^T$ is the DFT of the squared signal.

This result shows that if e is white noise then the expected power spectrum of the signal-correlated noise e_b is also flat. Moreover, the correlation between the elements of $F^H e_b$ depends solely on the Fourier transform of the squared signal; the more low frequent the signal $\overline{b}$, the narrower the effective bandwidth of $\mathrm{Cov}(F^H e_b)$ and therefore the more local the correlation between the elements of $F^H e_b$.

Hence we conclude that for the discrete ill-posed problem, where the signal b is indeed low frequent due to its origin as the results of an integration, the signal-correlated noise generated by the model (6.1) is practically white noise. Therefore it can be treated by the NCP method discussed in the previous section.

7 Numerical examples and tests.

As mentioned in the Introduction, the ultimate goal of this work is to produce a parameter choice rule that is computationally practical for large-scale problems. Therefore, in Section 7.1, we study the behavior of the NCP method for a representative, large-scale test problem in image deblurring. In Section 7.2, we study the performance of our rule vs. GCV, a well-known, statistically-motivated parameter choice rule, on a class test problems.

7.1 The NCP criterion for image deblurring problems.

Here we use a large-scale image deblurring problem from RESTORE TOOLS [12], where the coefficient matrix A represents the blurring, and the vectors $b = \mathrm{vec}(B)$ and $x = \mathrm{vec}(X)$ are "stacked" versions of the columns of the blurred image B and the exact image X, both of dimensions 256×256. We use the "satellite" image shown in Figure 7.2 below, and we create the noisy blurred image as $b = A\,x + e$ where e is white noise with noise level $\|e\|_2/\|A\,x\|_2 = 3{\cdot}10^{-2}$.

For the deblurring, we use the regularizing properties of the well-known, conjugate gradient least-squares (CGLS) method, i.e., we run CGLS on the original

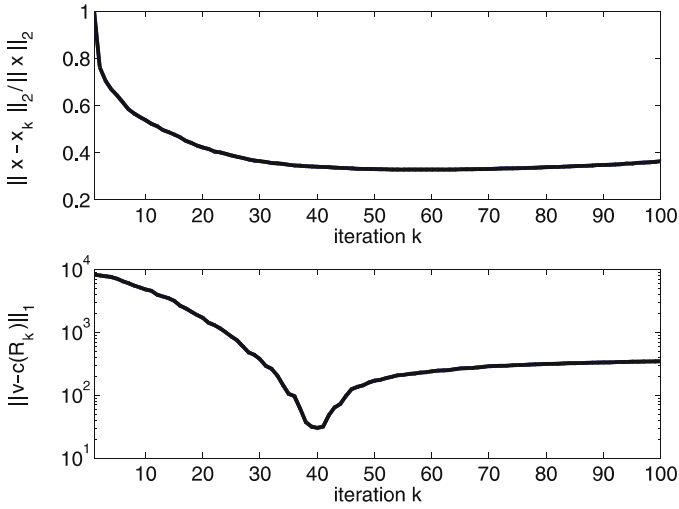

Figure 7.1: Top: the CGLS error history. Bottom: the quantity $\mathcal{N}_k$ in (7.1) which measures the maximum distance from the NCP to the straight line, for the 256×256 "satellite" image deblurring problem. The minimum of $\mathcal{N}_k$ occurs for $k = 40$.

problem (without regularization) and use the fact that for discrete ill-posed problems, the number k of iterations acts as a regularization parameter. This is a spectral filtering method, but the filter factors are never computed explicitly; see, e.g., Chapter 6 in [8] for more details. Each CGLS iterate x_k corresponds to a reconstructed image X_k such that $x_k = \mathrm{vec}(X_k)$. Similarly, the residual vector $r_k = A\,x_k - b$ corresponds to a residual image R_k such $r_k = \mathrm{vec}(R_k)$, and we should apply the 2D version of the NCP analysis to this residual image.

The top plot in Figure 7.1 shows the relative error $\|x - x_k\|_2/\|x\|_2$ in the kth iterate as a function of k, where $x = \mathrm{vec}(X)$ is the exact solution. For each CGLS iteration, we compute the residual image R_k and its NCP via the definition in (3.8) for 2D signals. The bottom plot in Figure 7.1 shows the deviation of $c(R_k)$ from a straight line, as measured by the quantity

$$\mathcal{N}_k = \|v - c(R_k)\|_1, \tag{7.1}$$

similar to Eq. (5.1). Clearly the quantity $\mathcal{N}_k$ is able to track the overall behavior of the error history quite well, and the minimum of $\mathcal{N}_k$ corresponds to a near-optimal solution. Figure 7.2 shows the exact image X, the blurred image B, the optimal reconstruction (for $k = 54$), and the reconstruction with $k = 40$ chosen by minimization of $\mathcal{N}_k$. Alternatively, we can use the smallest k for which the NCP lies within the Kolmogorov–Smirnoff limits; this leads to the choice $k = 38$. Both variants of the NCP method produce good reconstructions. We note that we ran a number of experiments with different noise realizations and different true images, and consistently found that both NCP-

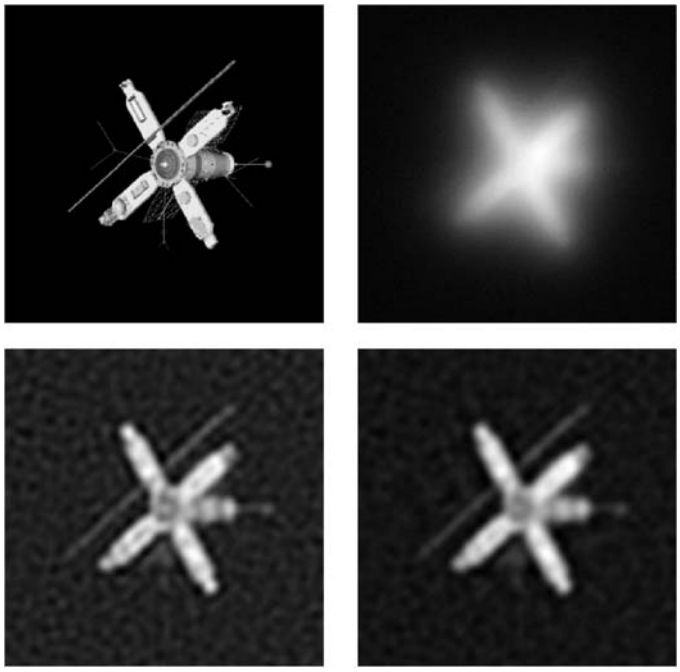

Figure 7.2: The 256×256 images in the "satellite" image deblurring problem. Top row: exact image and noisy blurred image. Bottom row: optimal reconstruction for $k = 54$ (left) and reconstruction for $k = 40$ chosen by minimization of $\mathcal{N}_k$ (right).

based parameter choice methods selected values which lead to restorations that were qualitatively very close to the one that was selected as optimal in the 2-norm.

7.2 Comparison with generalized cross validation.

To illustrate the robustness of our NCP-based method, we compare its performance with the GCV method which is another parameter-choice method rooted in a statistical formulation. We use eight different test problems:

1: `baart`	2: `shaw`	3: `wing`	4: `foxgood`
5: `gravity`	6: `heat`	7: `ilaplace`	8: `phillips`

and for each test problem we generate eight noise realizations with relative noise level 10^{-2}. The Tikhonov regularization parameter λ is computed by means of GCV as well as our new NCP-based method, using the largest λ for which the residual's NCP lies within the Kolmogorov–Smirnoff limits. We also compute the optimal regularization parameter λ^* which minimizes the error in the Tikhonov solution, i.e.,

$$\lambda^* = \operatorname{argmin} \|x - x_{\lambda^*}\|_2 / \|x\|_2,$$

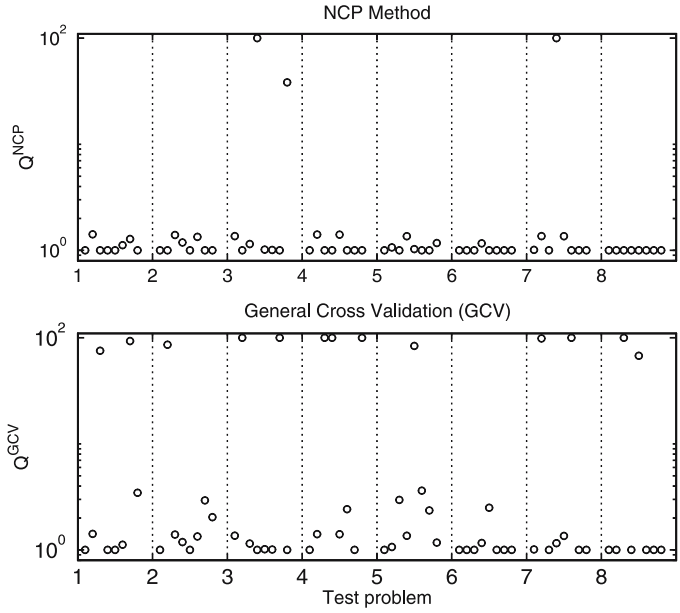

Figure 7.3: Comparison of the GCV and NCP-based parameter choice methods. For each test problem we create eight white noise realizations with relative noise level 10^{-2}. The two figures show the quality measures Q^{NCP} and Q^{GCP}. Both methods fail occasionally, but NCP fails fewer times than GCV. Moreover, the regularized solutions are, on the average, better for NCP than for GCV.

where x is the exact solution. The quality of all the regularized solutions is then measured by the quantity

$$Q^{\mathrm{M}} = \frac{\|x_\lambda - x\|_2}{\|x_{\lambda^*} - x\|_2}, \quad \mathrm{M} = \mathrm{GCV},\ \mathrm{NCP},$$

where M denotes the method use; the minimum value $Q^{\mathrm{M}} = 1$ is optimal, and any value $Q^{\mathrm{M}} > 100$ is considered off the scale.

The results of our comparison are summarized in Figure 7.3. We see that both GCV and NCP occasionally fail to give a good regularization parameter, but NCP fails fewer times than GCV. The occasional failure of GCV is a known difficulty associated with this method. An examination of the three cases where the new method fails reveals that the NCPs of the three random noise vectors e are very close to the Kolmogorov–Smirnoff limits – and hence our statistical test fails to identify a white-noise residual. The failures of both methods in these cases are consequences of these methods being based on a statistical assumption which is occasionally violated by the actual data. For those problems where the methods do not fail, the NCP-based method gives results which are, on the average, better than those from the GCV method. The displayed results are consistent with the results we obtained when we repeated

the experiment for noise levels of .1 and .01 percent, and therefore we do not include those figure here. We conclude that for these test problems, our new method is more robust and gives better results than GCV for realistic noise levels.

8 Conclusions and future work.

By exploring the relationship between the SVD and discrete Fourier bases for discrete ill-posed problems arising from the discretization of Fredholm integral equations, we have developed insight into how one can take advantage of residual components, rather than norms, to determine how and when signal is adequately separated from noise as a function of the regularization parameter. Our insight is valid for all regularization methods that can be implicitly expressed in terms of a filtered spectral expansion, including many iterative regularization methods that are particularly suited for large-scale problems.

While the insight depends on the SVD characterization of the spectral filtering, we emphasize that our analysis tools and our parameter-choice method do not – instead, we use the fast Fourier transform, which makes the method attractive for large-scale problems.

Our insight led us to a convenient parameter-choice method for the class of discrete ill-posed problems we consider that is based on the normalized cumulative periodogram. The core computational tool for our new method is the fast Fourier transform (FFT) which makes the method computationally attractive for large-scale problems. We illustrated the use of our method for problems with one- and two-dimensional solutions and white noise, and we showed that, in cases where the signal is predominantly low-frequent, the method can also be used in connection with noise that is correlated with the signal.

Acknowledgement.

The authors are very grateful to Jonathan Bihari for his assistance with Section 2.

REFERENCES

1. A. Boggess and F. Narcowich, *A First Course in Wavelets with Fourier Analysis*, Prentice Hall, New Jersey, 2001.
2. V. Faber, A. Manteuffel, A. B. White Jr., and G. M. Wing, *Asymptotic behavior of singular values and functions of certain convolution operators*, Comput. Math. Appl., 12A (1986), pp. 733–747.
3. W. A. Fuller, *Introduction to Statistical Time Series*, 2nd edn., Wiley, New York, 1996.
4. R. R. Goldberg, *Methods of Real Analysis*, 2nd edn., Wiley, New York, 1976.
5. P. C. Hansen, *Computation of the singular value expansion*, Computing, 40 (1988), pp. 185–199.
6. P. C. Hansen, *Analysis of discrete ill-posed problems by means of the L-curve*, SIAM Rev., 34 (1992), pp. 561–580.

7. P. C. Hansen, *Regularization Tools: A Matlab package for analysis and solution of discrete ill-posed problems*, Numer. Algorithms, 6 (1994), pp. 1–35.

8. P. C. Hansen, *Rank-Deficient and Discrete Ill-Posed Problems*, SIAM, Philadelphia, 1998.

9. P. C. Hansen, *Deconvolution and regularization with Toeplitz matrices*, Numer. Algorithms, 29 (2002), pp. 323–378.

10. M. E. Kilmer and D. P. O'Leary, *Choosing regularization parameters in iterative methods for ill-posed problems,* SIAM J. Matrix Anal. Appl., 22 (2001), pp. 1204–1221.

11. R. Kress, *Linear Integral Equations*, 2nd edn., Springer, Heidelberg, 1999.

12. J. G. Nagy, K. Palmer and L. Perrone, *Iterative methods for image deblurring: A Matlab object-oriented approach*, Numer. Algorithms, 36 (2004), pp. 73–93.

13. D. P. O'Leary, *Near-optimal parameters for Tikhonov and other regularization methods*, SIAM J. Sci. Comput., 23 (2001), pp. 1161–1171.

14. B. W. Rust, *Truncating the Singular Value Decomposition for Ill-Posed Problems*, Report NISTIR 6131, Mathematical and Computational Sciences Division, NIST, 1998.

15. A. M. Urnamov, A. V. Gribok, H. Bozdogan, J. W. Hines, and R. E. Uhrig, *Information complexity-based regularization parameter selection for solution of ill conditioned inverse problems*, Inverse Probl., 18 (2000), pp. L1–L9.

16. G. Wahba, *Spline Models for Observational Data*, SIAM, Philadelphia, 1990.